# Comparative Analysis on the Mechanical Properties of Mortise-Tenon Joints in Heritage Timber Buildings with and without a 'Que-Ti' Component

Yuanhe Li, Lihong Yao,* Yu Guo, Ruijng Liu, Yueqi Wu, Honglei Jia, Xia Yu, Ce Wang, Zhibang Hu, and Chang Chen

Three kinds of typical Chinese traditional mortise-tenon joints were tested. The effects of sparging on the deformation, hysteretic behavior, strength and stiffness degradation, and energy dissipation of the mortise-tenon joints were studied *via* low-cycle reversed loading tests with and without a 'Que-Ti' component. The results showed the following: the bearing capacity of the straight-tenon joint was the strongest, and the hysteretic loop of the through-tenon joint and half-tenon joint were asymmetric due to the asymmetry of the tenon form. The half-tenon joint was most likely to pull out the tenon, and the tenon pulling condition of the half-tenon joint can be effectively alleviated by adding a 'Que-Ti' component. From the perspective of energy consumption, it was found that the energy consumption capacity of the mortise-tenon joints after adding a 'Que-Ti' component was stronger than the joints without a 'Que-Ti' component. This shows that the 'Que-Ti' can be used as an effective component in terms of enhancing the mechanical properties of the mortise-tenon joints.

*DOI: 10.15376/biores.17.3.4116-4135*

*Keywords: Heritage timber buildings; 'Que-Ti' component; Mortise-tenon joints; Hysteretic behavior*

*Contact information: College of Material Science and Art Design, Inner Mongolia Agricultural University, Hohhot 010018 P.R. China; *Corresponding author: yaolihong82@163.com*

## INTRODUCTION

A 'Que-Ti' is a special component in heritage timber buildings that plays the role of both a mechanical and decorative component. It is a short wood piece placed under a beam and at the intersection of a column (Lyu *et al.* 2016). A 'Que-Ti' is usually placed at the intersection of the horizontal material (beam, *i.e.*, Fang) and the vertical material (column) of heritage timber buildings, and generally, it has three roles: the first is to shorten the net span of the beam to enhance the bearing capacity (Lyu *et al.* 2017); the second is to reduce the downward shear force between the beam and column (Dai 2020); and the third is to prevent the angle tilt between the horizontal and vertical wooden components (Yang *et al.* 2020). The development of the configuration of the 'Que-Ti' began to take shape during the Northern Wei Dynasty, and it was not until the Ming Dynasty that it began to be widely used and became a unique heritage timber building component in the Qing Dynasty (Chun *et al.* 2019).

A 'Que-Ti' component is assembled using the mortise-tenon connection technology in heritage timber buildings. It is the combination of structural mechanics and aesthetics, for it reinforces the mechanical properties of the mortise-tenon joints connecting the Fang and the column in terms of the structural mechanics as well as the shaping of the

wings attached to both sides of the column cap with interesting contour curves, paints, and carvings at an artistic level (as shown in Fig. 1) (Li *et al.* 2020).

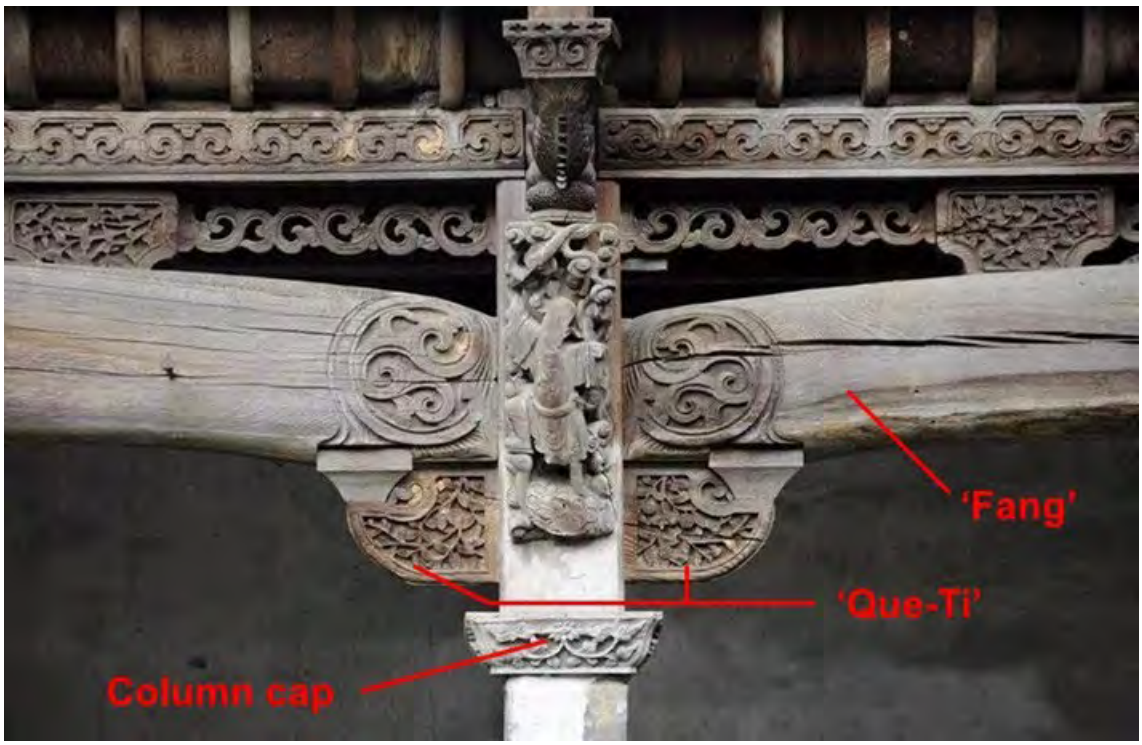


**Fig. 1.** A 'Que-Ti' component in heritage timber building

The mortise-tenon joint in heritage timber architecture is usually considered as a semi-rigid joint in modern structural engineering, and the primary reason it is a research focus by many scholars is due to its excellent seismic performance (Xue *et al.* 2018, 2019). Taking the bending moment capacity of the mortise-tenon joint as the starting point for research is an important means to measure the strength of the mortise-tenon joint and evaluate its seismic performance. Generally, the factors affecting the bending moment capacity and bending stiffness of mortise-tenon joints are the wood species, growth ring, adhesive type, load type, tenon size, tenon geometry, *etc.* (Záborský *et al.* 2017; Hu and Liu 2020). Considering the effects of the wood species, adhesive type, and tenon size on the bending strength and flexibility of a T-shaped mortise-tenon joint, the test showed that the stiffness of the mortise-tenon joint was positively correlated with the tenon length and width, and the influence of the tenon width was more obvious than that of the length (Erdil *et al.* 2005). Taking into account the function of the tenon geometry, grain orientation, length, and shoulder fit, the bending moment capacity of the mortise-tenon joint with complete insertion of the tenon was 54% larger than the bending moment capacity of the joint without complete insertion. Additionally, a rectangular tenon has the largest bending moment capacity under the same conditions (Likos *et al.* 2012). In terms of the influence of the joint dimensions on the mechanical properties of the mortise-tenon joint, regression functions in the form of a second power polynomial with interactions or in the form of a power functions product can be used to express the relationship, and the influence on the joint strength from strong to weak is the tenon length, tenon width, and tenon thickness, respectively (Wilczyński and Warmbier 2003; Tankut and Tankut 2005). In addition,

experiments have shown that the shape of the adhesive has a strong influence on the strength of the tenon, and non-dilatational deformation can considerably limit the pressure of the tenon on the mortise, thereby reducing the level of dangerous shear stresses (Prekrat and Smardzewski 2010).

The mortise-tenon joint is the weakest part and has a great influence on the mechanical properties of heritage timber buildings; therefore, analyzing the damage of mortise-tenon joint under seismic waves in terms of their strength, stiffness, and energy dissipation is an important method to evaluate the seismic performance of heritage timber buildings (Poletti *et al.* 2019). A specific research method is to use finite element analysis software or physical tests to analyze the dynamic response of a mortise-tenon joint under different seismic intensities to extract the moment-rotation ($M$-$\theta$) curve of the mortise-tenon joint before and after damage, and to measure the energy dissipation of the mortise-tenon joint with the area of the largest hysteresis loop as the quantitative indicator (Wang and Jin 2014; Xie *et al.* 2020). To effectively simulate the seismic performance of mortise-tenon joints, it is necessary to accurately evaluate the load-deformation hysteretic performance of the joints (Xie *et al.* 2019). To achieve this evaluation, it is necessary to establish the hysteretic models of the mortise-tenon joints, where the existing hysteretic models of mortise-tenon joints can be divided into three categories, *i.e.*, finite element (FE) models, physical models, and phenomenological models (Xue and Xu 2018; Meng *et al.* 2019). The finite element models and physical models can effectively predict the hysteretic performance of mortise-tenon joints but are not suitable for the structural model with a large number of joints (Loss *et al.* 2018). However, the phenomenological models are controlled by a set of mathematical equations with parameters to specify the envelope path and hysteresis so that the application scope is wider and can be used in combination with open-source software (Dong *et al.* 2021).

When utilizing mortise-tenon technology to connect the components of heritage timber structures, the mortise-tenon joint is formed by inserting different shapes of tenons into the corresponding mortise, and the typical mortise-tenon joints concluded from various joint forms include straight-tenon, through-tenon, half-tenon, swallowtail-tenon, *etc.* (Huang *et al.* 2017). Long-term stress at the mortise-tenon joints will lead to joint loosening and tenon pull-out, which could moderately weaken the stiffness, bearing capacity, and energy dissipation capacity of heritage timber structures. Therefore, it is of great scientific importance to compare the mechanical properties of different types of mortise-tenon joints (Yue 2014). In this paper, three typical mortise-tenon joints, *i.e.*, straight-tenon, through-tenon, and half-tenon, were selected as the research objects. Each mortise-tenon joint pattern was made into two types: one type assembled with the 'Que-Ti' component and the other type without. The influence of the 'Que-Ti' component on the mechanical properties of the mortise-tenon joint was compared and analyzed from four aspects, *i.e.*, the hysteretic curve, skeleton curve, force and stiffness, and energy dissipation (Chun *et al.* 2011).

## EXPERIMENTAL

### Mechanical Property Tests of *Pinus sylvestris var. mongolica*

The standard values of the bending strength, modulus of elasticity, compressive strength parallel to the grain, full surface compressive strength perpendicular to the grain (tangential direction and radial direction), and sectional compressive strength perpendicular to the grain (tangential direction and radial direction) were obtained by

testing the mechanical properties of *Pinus sylvestris* var. *mongolica*. The experiments were carried out according to the test specifications outlined by GB/T standard 1936.1 (2009), GB/T standard 1935 (2009), and GB/T standard 1939 (2009). In this part of the test, the measured values of each index were obtained according to the average values obtained after the test of 15 specimens.

The specific processing of the material test is shown in Fig. 2, where (a) is the test process of the modulus of rupture, (b) is the test process of the compressive strength parallel to the grain, (c) is the test process of the full surface compressive strength perpendicular to the grain, and (d) is the test process of the sectional compressive strength perpendicular to the grain. The standard values of all the mechanical properties tested are shown in Table 1.

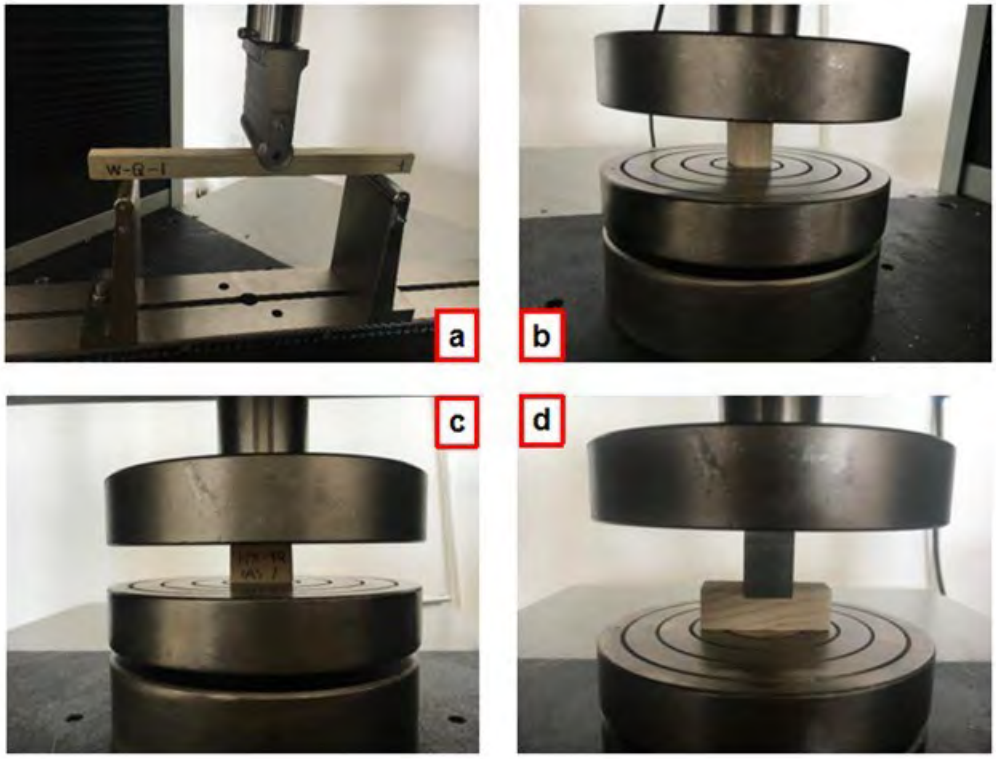


**Fig. 2.** The specific test process of *Pinus sylvestris var. mongolica*: (a) test process of the modulus of rupture; (b) test process of the compressive strength parallel to the grain; (c) test process of the full surface compressive strength perpendicular to the grain; and (d) test process of the sectional compressive strength perpendicular to the grain

**Table 1.** Physical and Mechanical Parameters of *Pinus sylvestris var. mongolica*

| Physical Parameters | | Mechanical Parameters | | | | | | |
|---|---|---|---|---|---|---|---|---|
| D (g/cm$^3$) | MC (%) | MOR (MPa) | MOE (MPa) | CS-L (MPa) | FSC-R (MPa) | FSC-T (MPa) | SCS-R (MPa) | SCS-T (MPa) |
| 0.49 | 11 | 59.48 | 6078.92 | 35.20 | 5.14 | 5.27 | 3.11 | 2.99 |

Note. D: density; MC: moisture content; MOR: Modulus of rupture; MOE: Modulus of elasticity; CS: compressive strength parallel to the grain; FSC: full surface compressive strength perpendicular to the grain; SCS: sectional compressive strength perpendicular to the grain; L: longitudinal direction; R: radial direction; and T: tangential direction

## Design and Fabrication of the Specimens

The fabrication of the specimens was based on the Cai and Fèn system (1 Cai = 15 Fèn) stipulated in *Ying Zao Fa Shi*, Song Dynasty. In the Cai and Fèn system, there are eight grades (Grade I to Grade VIII) of Cai, and this paper takes Grade III, in which a Fèn is approximately equal to 16 mm. The specimens were designed at a 1 to 3.2 scale ratio to ensure both moderate size and integral geometric dimensions of the components. In the experiment, three types of mortise-tenon joint specimens, *i.e.*, straight-tenon joints, through-tenon joints, and half-tenon joints, were made. Two specimens were made for each type of mortise-tenon joint, one of which was supported by a 'Que-Ti' component and the other was not, for a total of six specimens. All specimens were made of *Pinus sylvestris* var. *mongolica*, and the basic mechanical properties of *Pinus sylvestris* var. *mongolica* were tested.

The mortise-tenon joint specimens without a 'Que-Ti' component are composed of two parts: the column and the Fang, while the mortise-tenon joint specimens with a'Que-Ti' component were composed of three parts: the column, the Fang and the 'Que-Ti' (Fig. 3.). The basic dimensions of the 'Que-Ti' component were 63 mm x 180 mm x 450 mm (width, height, and length), and the tenon of the 'Que-Ti' component was 15 mm x 135 mm x 75 mm (width, height, and length), while the other dimensions of each mortise-tenon joint are shown in Table 2.

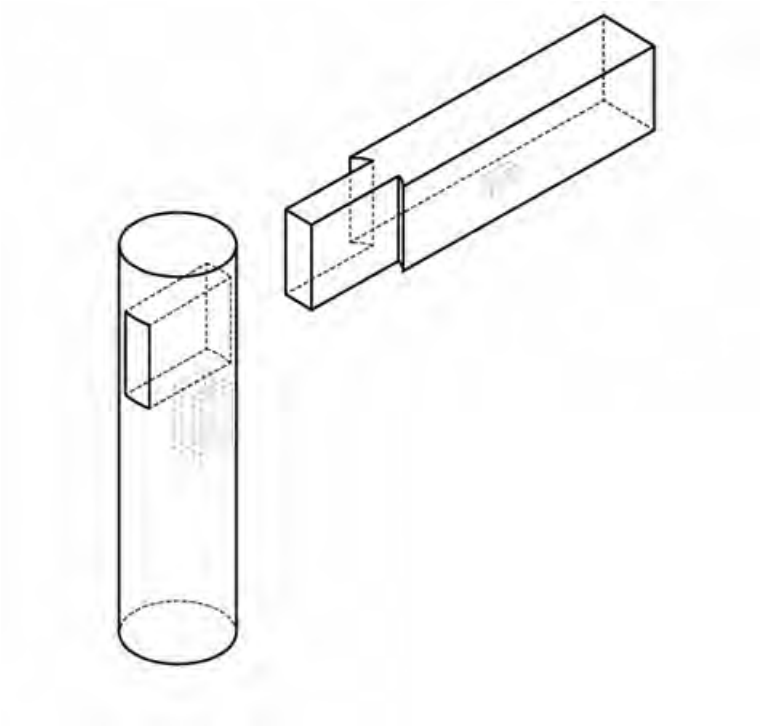

**(a)** Straight-tenon joint

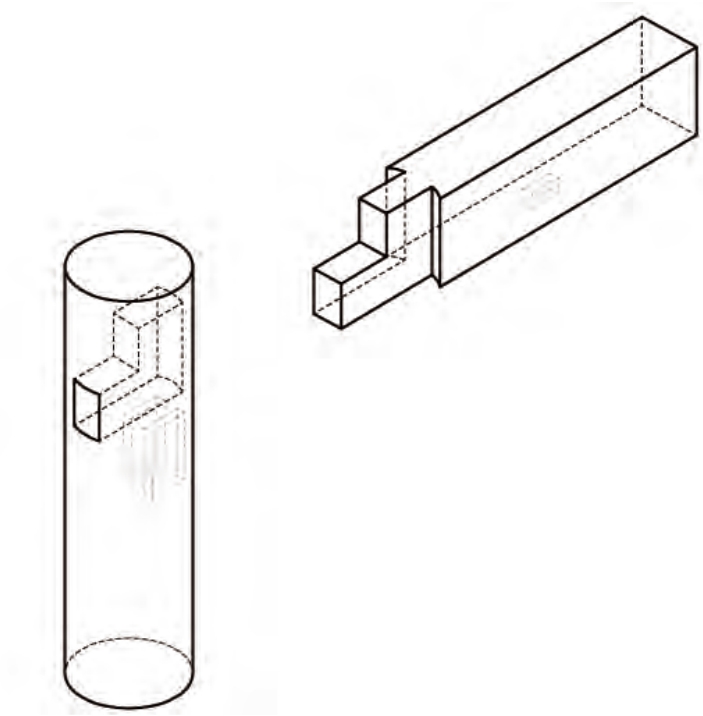

**(b)** Through-tenon joint

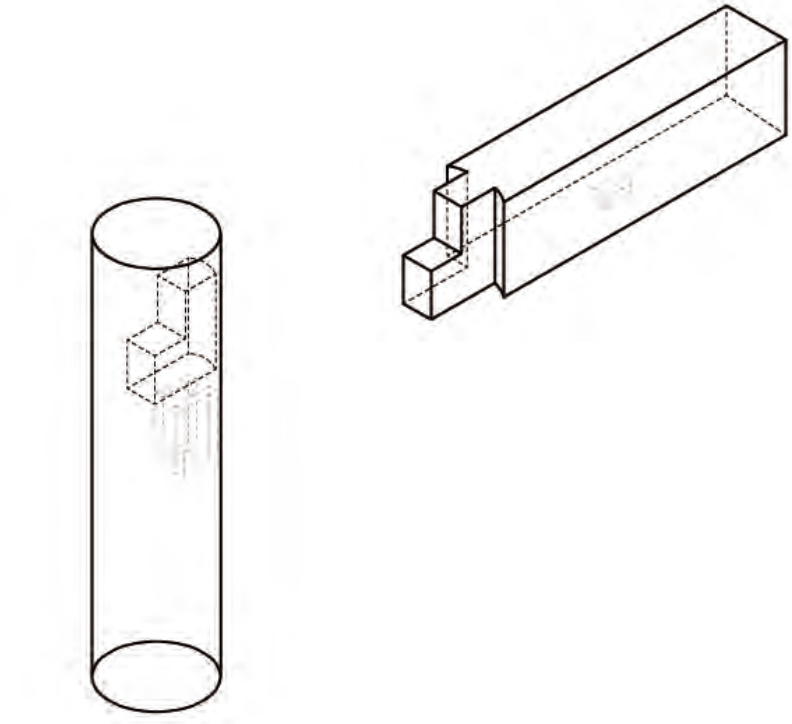

**(c)** Half-tenon joint

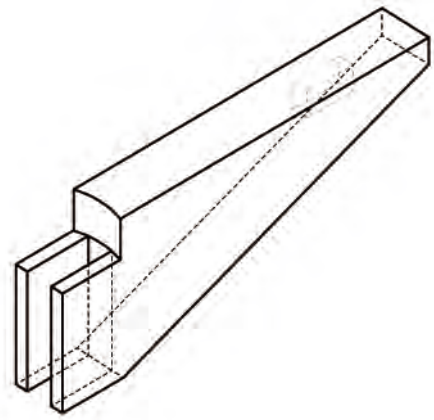

**(d)** 'Que-Ti' component

**Fig. 3.** The three types of mortise-tenon joints in the experiment

**Table 2.** Basic Dimensions of Each Mortise-Tenon Joint

| Member | Part name | Prototype (Fèn) | Straight-tenon Joint (mm) | Through-tenon Joint (mm) | Half-tenon Joint (mm) |
|---|---|---|---|---|---|
| Column | Diameter | 42 | 210 | 210 | 210 |
| Fang | Height | 36 | 180 | 180 | 180 |
| | Width | 24 | 120 | 120 | 120 |
| Tenon | Tenon big-head height | 36 | 180 | 180 | 180 |
| | Tenon small-head height | | | 90 | 90 |
| | Tenon width | 12 | 60 | 60 | 60 |
| | Tenon big-head length | 42 | 210 | 210 | 140 |
| | Tenon small-head length | | | 105 | 70 |

## Loading Equipment

A low-cycle reversed loading test was carried out by an electronic universal testing machine (Model: WDW-T100; Jinan Tianchen Testing Machine Manufacturing Co., Ltd., Jinan, China), which was primarily equipped with imported AC servo motors and a speed control system (as shown in Fig. 4.).

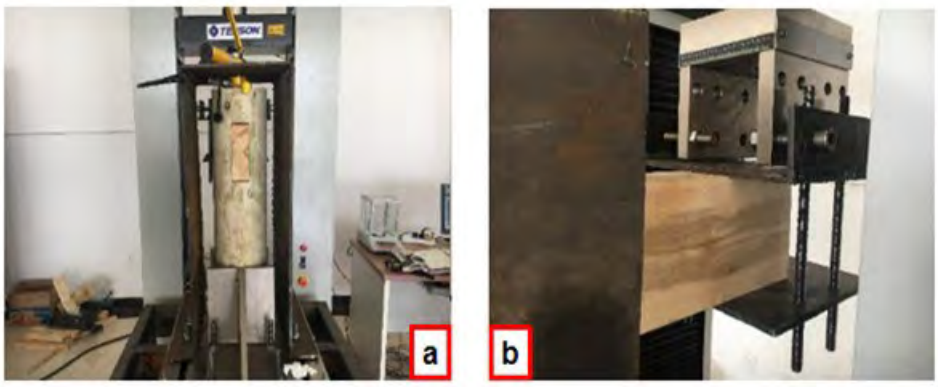


**Fig. 4.** Loading equipment: (a) electronic universal testing machine; and (b) fixation of specimen

The maximum output force of the electronic universal testing machine was 100 KN, the relative displacement error was ± 0.5%, and the maximum stroke was 2 m. The actuator was connected to the end of the mortise-tenon joint specimen through bolts and steel plates, and the specimens were subjected to low-cycle reversed loading.

## Loading Scheme

In the test, the column bottom of the specimen was fixed on the test device, and the vertical load on the top of the column was simulated by applying a 13.5 KN vertical load through the jack. Then, the vertical low-cycle reversed loading was carried out from the loading point on the Fang component at the top of the specimen through the actuator of the universal mechanical testing machine.

According to the ISO standard 16670 (2003), the loading scheme was controlled by changing the displacement amplitude. The distance between the actuator and the upper edge of the column was 570 mm, while the control displacement (the control displacement values of the 6 joints obtained *via* monotonic loading test are shown in Table 3) was the ultimate displacement determined by the unidirectional loading test (the ultimate displacement was taken as the displacement when the load decreased to 80% of the ultimate load during the test or the tenon joint was seriously damaged). First of all, 1.25%, 2.5%, 5%, 7.5%, and 10% of the control displacement value were used for the single cyclic pre-loading, and then 20%, 40%, 60%, 80%, 100%, and 120% of the control displacement value were used for the three cyclic loading tests. The specific loading system is shown in Fig. 5. The partial experimental phenomena of the low-cycle reversed loading test are shown in Fig. 6.

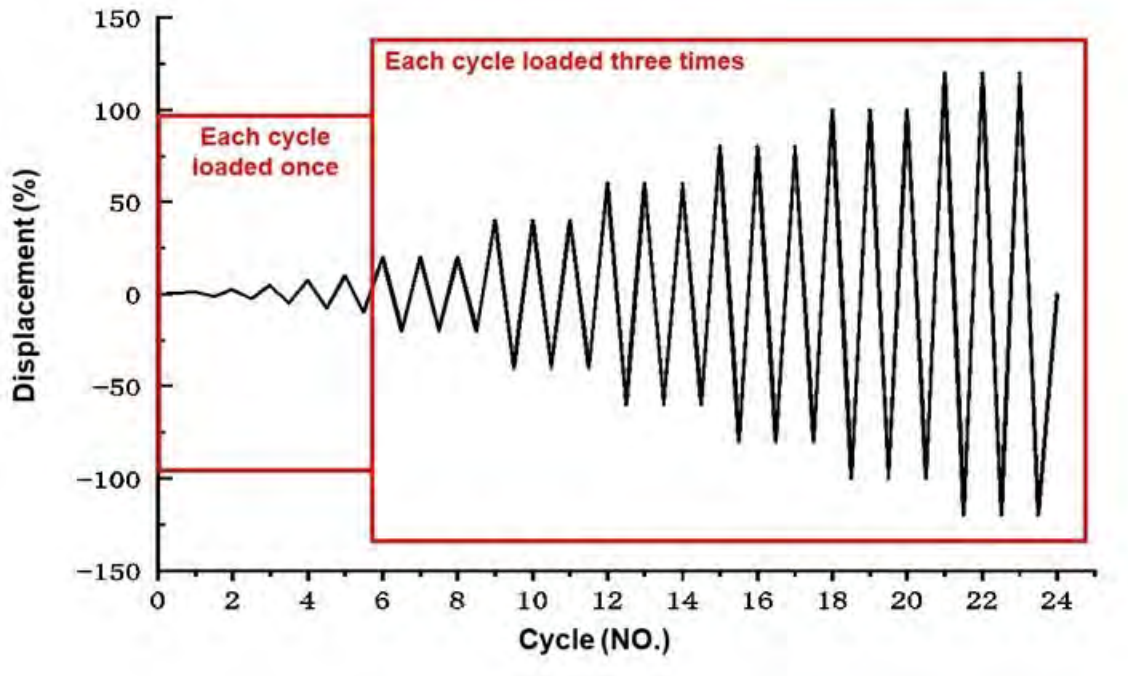


**Fig. 5.** Loading scheme

**Table 3.** Control Displacement of Each Mortise-tenon Joint

| Specimen Name | DZ-1 | ST-1 | SB-1 | DZ-2 | ST-2 | SB-2 |
|---|---|---|---|---|---|---|
| Control Displacement (mm) | 73.21 | 76.38 | 84.39 | 88.38 | 87.67 | 91.68 |
| Note. DZ-1: straight-tenon joint without a 'Que-Ti'; DZ-2: straight-tenon joint with a 'Que-Ti'; ST-1: through-tenon joint without a 'Que-Ti'; ST-2: through-tenon joint with a 'Que-Ti'; SB-1: half-tenon joint without a 'Que-Ti'; and ST-2: half-tenon joint with a 'Que-Ti' | | | | | | |

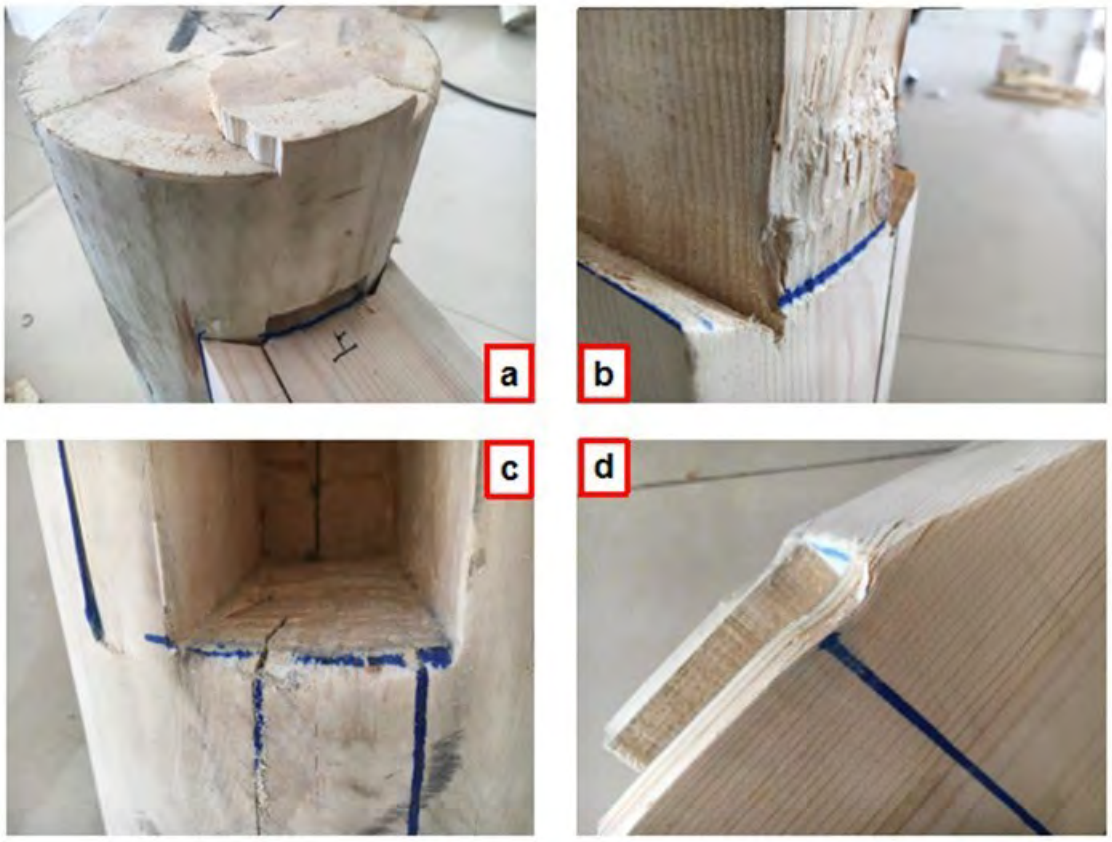


**Fig. 6.** Experimental phenomena: (a) splitting of the Fang; (b) damage of the tenon; (c) damage of the mortise; and (d) damage of the 'Que-Ti'

## RESULTS AND DISCUSSION

### Moment-rotation (M-θ) Hysteretic Curves

A moment-rotation hysteretic curve, also known as a moment-rotation restoring force curve, is a load displacement relationship curve obtained under reversed loading. The moment-rotation hysteretic curve of a mortise-tenon joint can reflect its energy dissipation, structural failure form, bearing capacity, stiffness, and strength degradation under reversed loading, which is a comprehensive evaluation method and basis for seismic performance. Generally, hysteresis curves can be divided into four types: shuttle-shape, arch-shape, anti-S-shape, and Z-shape. The load displacement relationship of each joint in this test was obtained *via* low-cycle reversed loading.

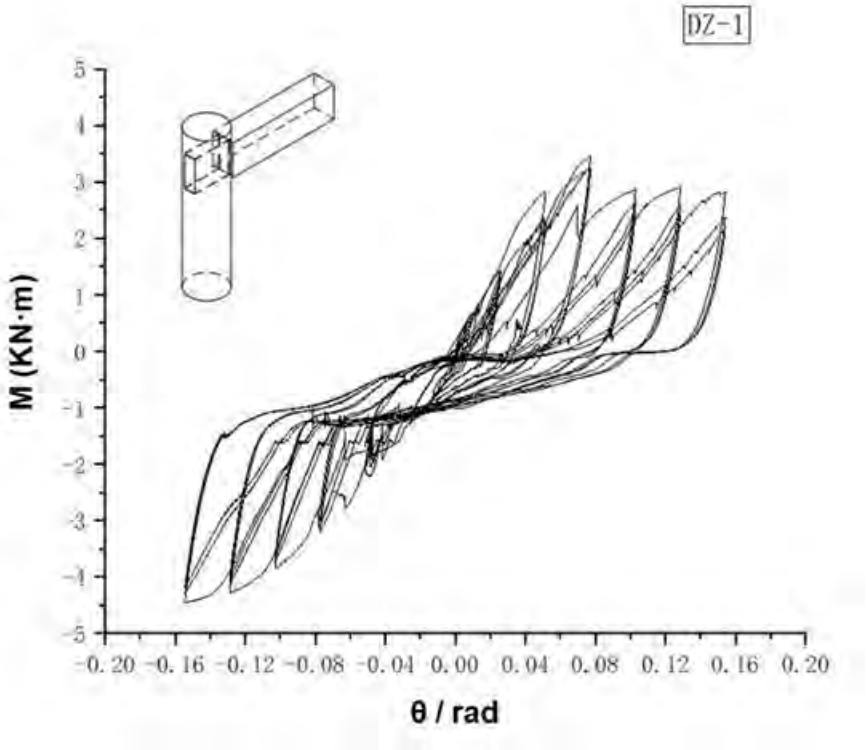


**(a)** Straight-tenon joint without a 'Que-Ti'

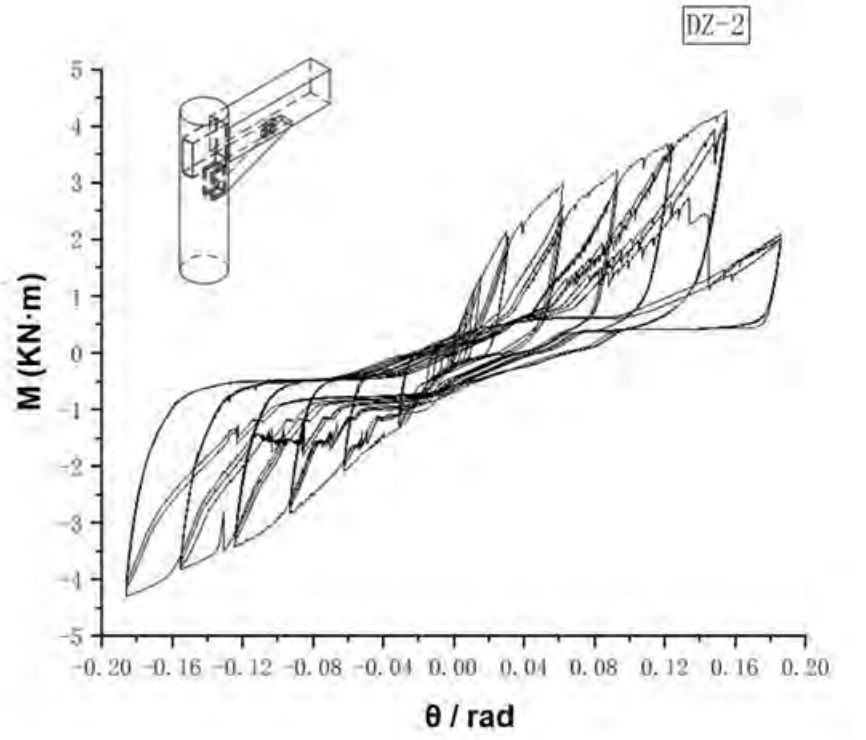


**(b)** Straight-tenon joint with a 'Que-Ti'

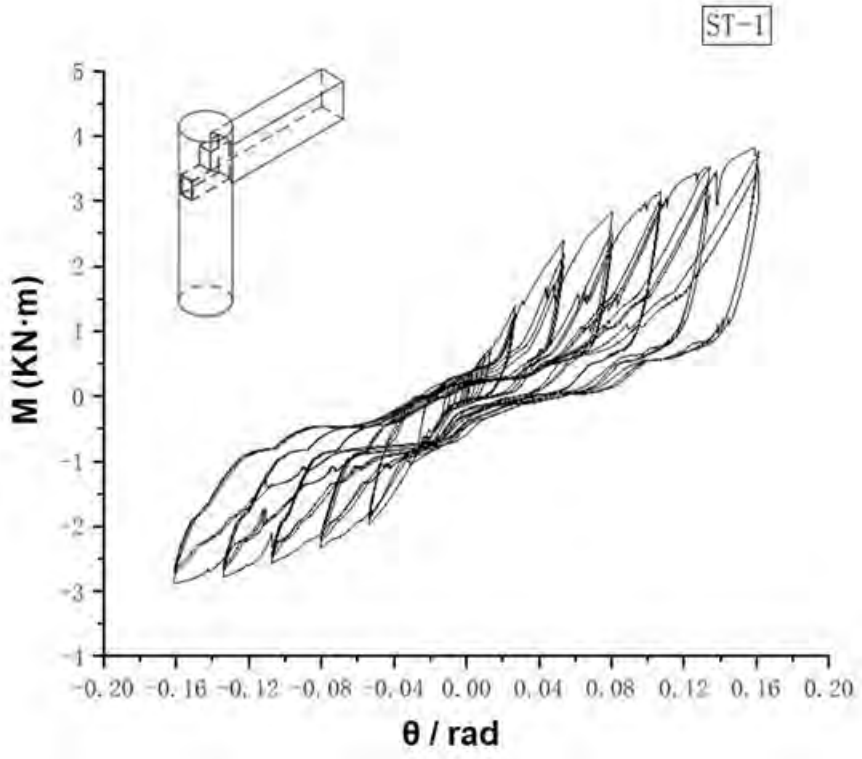


**(c)** Through-tenon joint without a 'Que-Ti'

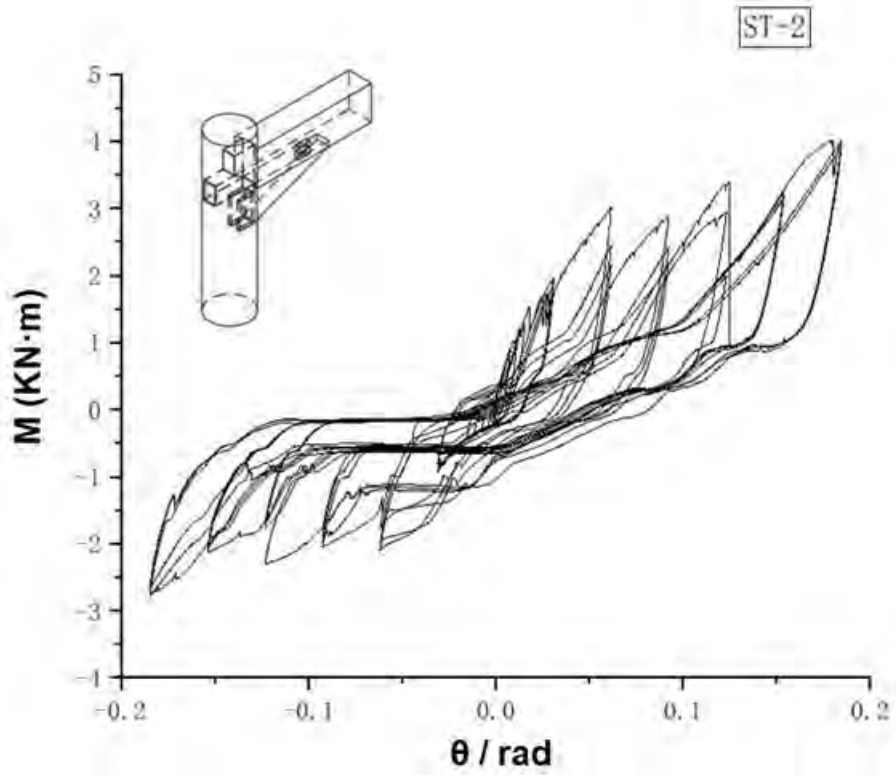


**(d)** Through-tenon joint with a 'Que-Ti'

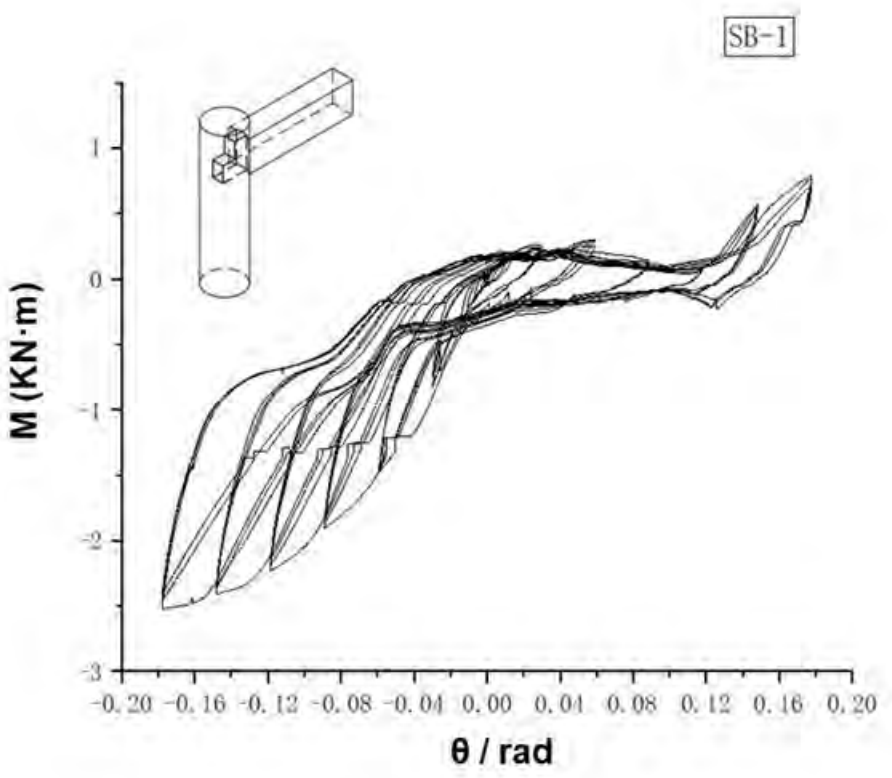


**(e)** Half-tenon joint without a 'Que-Ti'

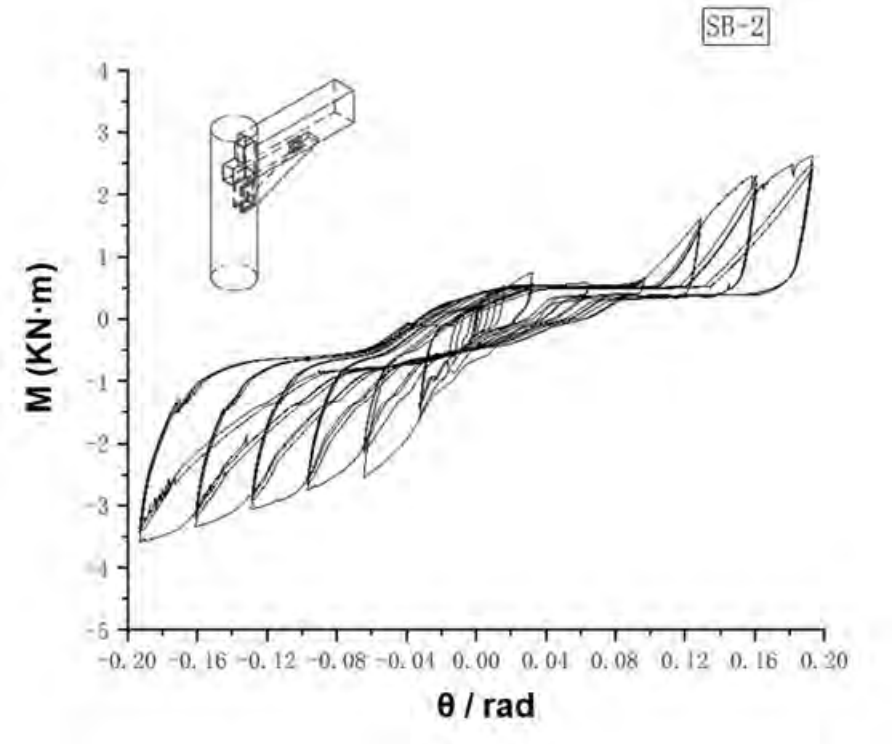


**(f)** Half-tenon joint with a 'Que-Ti'

**Fig. 7.** The moment-rotation (*M-θ*) hysteretic curves of the six mortise-tenon joints

As a whole, the moment-rotation ($M$-$\theta$) hysteresis curves of the six mortise-tenon joints (Fig. 7) in the test are similar to the inverted 'S' shape, and the overall pinching effect is obvious, which reflects that the mortise-tenon joints have a large slip phenomenon during the loading process.

As shown in the hysteretic curve of the unidirectional straight-tenon joint DZ-1 (Fig. 7a), the peak value decreased after the third order amplitude displacement under reversed loading. This was due to the continuous compression and pressure on the mortise and tenon during the long-term repeated staggered movement of the mortise-tenon joint, which led to wood splitting failure under the third order amplitude displacement control loading, and the performance of the mortise-tenon joint sharply dropped. In the path of the hysteretic loop, some uneven jitter could be observed, which was caused by the friction between the tenon and mortise, uneven fiber of the mortise and mortise, and the staggered movement of the tenon. Moreover, in the later stage of the test, the bending moment of specimen DZ-2 (Fig. 7b) obviously increased.

The asymmetry between the forward loading curve and reverse loading curve of ST-1 (Fig. 7c) and SB-1 (Fig. 7e) was obvious, which was consistent with the asymmetry of the tenon shape. There were joints in the long tenon of the through-tenon joint ST-1 (Fig. 7c), which was one of the reasons that the hysteretic loop of ST-1 under reverse loading was considerably larger than that under forward loading. The results showed that the pinch effect of SB-1 (Fig. 7e) was obvious, and the slip was serious, which was due to the small contact area between the tenon and mortise, and the tenon mortise was not fully squeezed during loading.

In addition, because of the small contact area between the tenon and mortise, the tenon pulling phenomenon was obvious in the initial loading stage. The overall hysteretic curve area was small, the energy consumption was small, and the asymmetry of the forward and reverse loading was obvious. From the hysteretic curve of specimen SB-2 (Fig. 7f), it could be found that the hysteretic loop surface under forward loading was caused by the upward reaction of the displacement, and the value was obviously smaller than the value under reverse loading.

The hysteretic area of the straight-tenon joints (DZ-1 and DZ-2) and through-tenon joints (ST-1 and ST-2) were obviously larger, which indicated that the greater the contact area between the tenon and mortise joint, the greater the bending moment that would be produced. Under the same rotation angle, the reaction force of the tenon was larger, so the area enveloped by the load displacement was larger. The hysteretic curves of the joints with a ‘Que-Ti’ component were obviously plumper, which indicated that the ‘Que-Ti’ component had a positive effect on the mechanical properties of the joints.

## Moment-rotation (M-θ) Skeleton Curves

A skeleton curve is the envelope line formed by the peak point of the first cycle of each loading stage when the specimen model is under cyclic loading, which can reflect the deformation status and characteristic properties of the mortise tenon joint model in different stress stages. Normally, the skeleton curves of mortise-tenon joints can be divided into the following stages: the elastic stage, the yield stage, the strengthening stage, and the failure stage.

According to Fig. 8, the skeleton curve of each mortise-tenon joint had a large slope at the initial loading stage, which was caused by the elastic working stage of the mortise-tenon joint. With the increase of the displacement amplitude, the angle increased, the

extrusion between the tenon and mortise increased, and the slope of curve correspondingly increased. As the test continued, with the increase of the displacement amplitude, the extrusion force between the mortise and tenon groove increased, the plastic deformation between the mortise and tenon gradually increased, the mortise and tenon joint became loose, and the slope of the curve decreased. The mortise-tenon joint began to gradually yield and entered the yield stage. When the rotation angle reached 0.08 rad, the growth of the node skeleton curve was slow, even the peak point appeared, reaching the strengthening stage. In the later stage of loading, as a whole, the curve was gentle, and some joint curves obviously decreased, and entered the failure stage.

As shown in Fig. 8, it could be determined that the bending moment of DZ-2 was considerably higher than the bending moment of DZ-1. At the beginning of loading, the slope of the DZ-2 skeleton curve was greater than the slope of the DZ-1 skeleton curve under positive loading. The bearing capacity of the DZ-2 specimen with a 'Que-Ti' under forward loading was considerably greater than the bearing capacity of DZ-1, which indicated that the 'Que-Ti' component offered upward force. The skeleton curves of the straight-tenon joints with and without a 'Que-Ti' were basically the same, which indicated that the 'Que-Ti' component had little effect on the bearing capacity of this type of joint, and tenon was the primary bearing part under loading.

The bending moments of the half-tenon joint with a 'Que-Ti' (SB-1) and without a 'Que-Ti' (SB-2) were obviously different, which indicated that the 'Que-Ti' component had considerable influence on the mechanical properties of this type of joint. In general, the joints with the 'Que-Ti' component could obviously produce a larger bending moment.

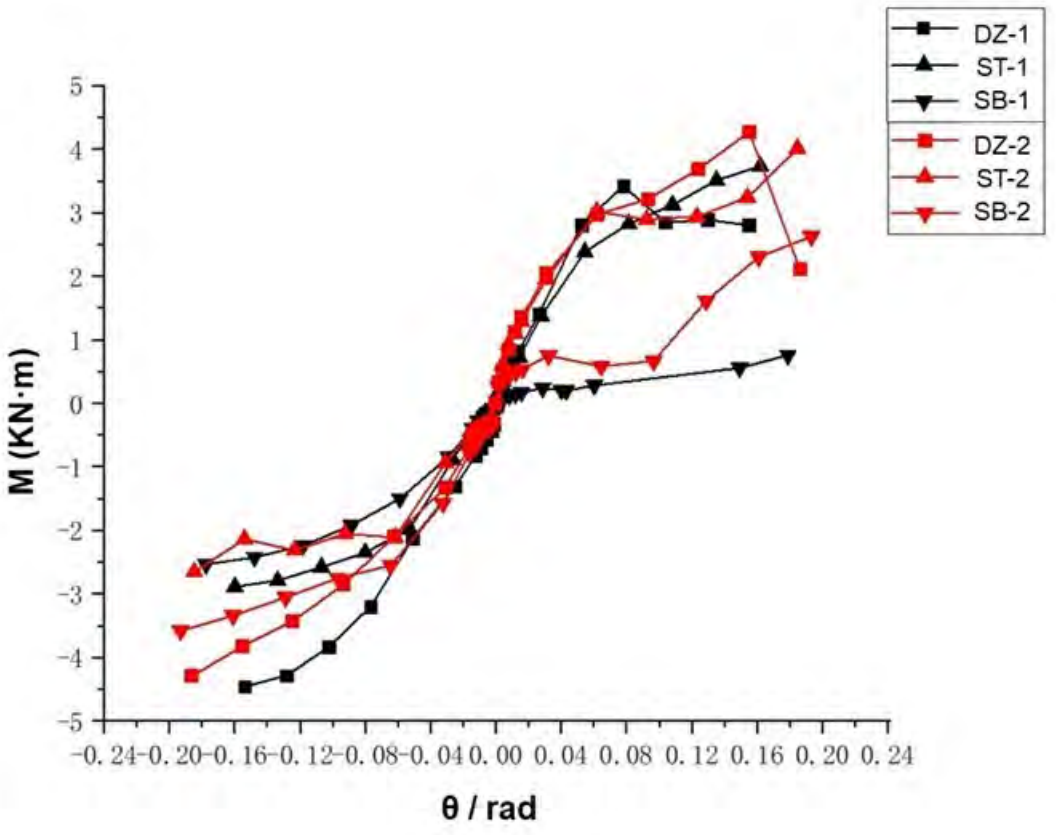


**Fig. 8.** The moment-rotation (M-θ) skeleton curves of the mortise-tenon joints

## Stiffness Degradation Curves

The stiffness of the mortise-tenon joint specimen is related to the number of loading cycles. With the increase of the number of loading cycles, the stiffness of the joint decreases, which is called stiffness degradation. The stiffness value of the specimen can be expressed by the secant stiffness under the same level of deformation, and the secant stiffness ($K_i$) of the joint is calculated according to Eq. 1,

$$K_i = \frac{|+F_i|+|-F_i|}{|+X_i|+|-X_i|} \quad (1)$$

where $+F_i$ is the bending moment of the positive peak point under the i$^{th}$ control displacement cyclic loading, $-F_i$ s the bending moment of the reverse peak point under the i$^{th}$ control displacement cyclic loading, $+X_i$ is the angle value of forward peak point under the i$^{th}$ control displacement cyclic loading, and $-X_i$ is the angle value of reverse peak point under the i$^{th}$ control displacement cyclic loading.

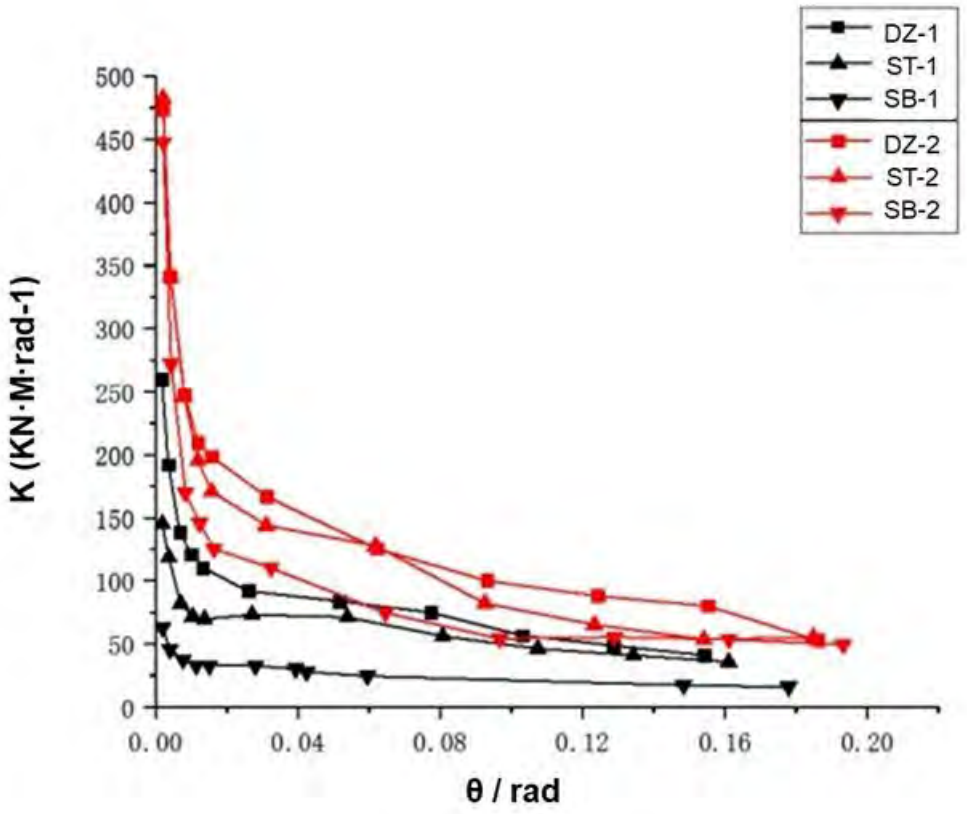


**Fig. 9.** The stiffness degradation curves of the mortise-tenon joints

According to the overall trend shown in Fig. 9, the stiffness of each mortise-tenon joint showed a gradual downward trend, and the initial stiffness of the joint was relatively large. After 0.01 rad, the curve decreased slowly and tended to be gentle.

From the stiffness degradation curve of the half-tenon joint, it could be seen that the initial stiffness of the half-tenon joint had a very obvious strengthening effect after adding the 'Que-Ti' component. In the test results of the mortise-tenon joint without a 'Que-Ti' component, the initial stiffness of the half-tenon joint was the smallest. This indicated that the 'Que-Ti' contributed the most to the tenon of the half-tenon joint.

The stiffness degradation law of the six types of mortise-tenon joint specimens was almost the same, and all of them showed a sharp decrease at first and then tended to be gentle with the increase of the rotation angle.

As shown in Fig. 9, the stiffness degradation curves of each mortise-tenon joint with and without the 'Que-Ti' component could be compared and analyzed. As a whole, the stiffness values of the tenon-mortise joints after adding the 'Que-Ti' were considerably improved, but the stiffness degradation trend was not very different. From a stiffness point of view, the stiffness values of the three types of mortise-tenon joints were increased to varying degrees after adding a 'Que-Ti', and the contribution of the 'Que-Ti' component to the three types of mortise-tenon joints was as follows: the half-tenon joint was greater than the through-tenon joint, which was greater than the straight-tenon joint.

## Energy Dissipation

The energy dissipation capacity of the mortise-tenon joint model is measured by the area surrounded by the bending moment rotation hysteresis loop, *i.e.*, the equivalent viscous damping coefficient (Fig. 10). The equivalent viscous damping coefficient of energy dissipation is usually used to evaluate the energy dissipation capacity. The larger the equivalent viscous damping coefficient is, the stronger the energy dissipation capacity is, which is calculated according to Eq. 2,

$$h_e = \frac{1}{2\pi} \times \frac{S_{(ABC+CDA)}}{S_{(OBE+ODF)}} \quad (2)$$

where $S_{(ACD+CDA)}$ is the area surrounded by the moment-rotation hysteresis loop, and $S_{(OBE+ODF)}$ is the sum of the area of triangle OBE and triangle ODF.

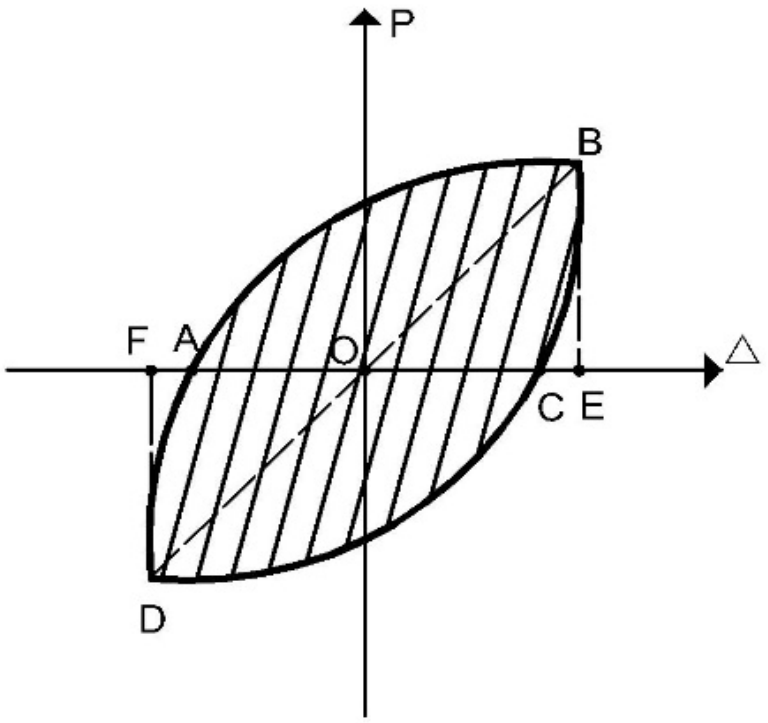


**Fig. 10.** Diagram of the equivalent viscous damping coefficient calculation

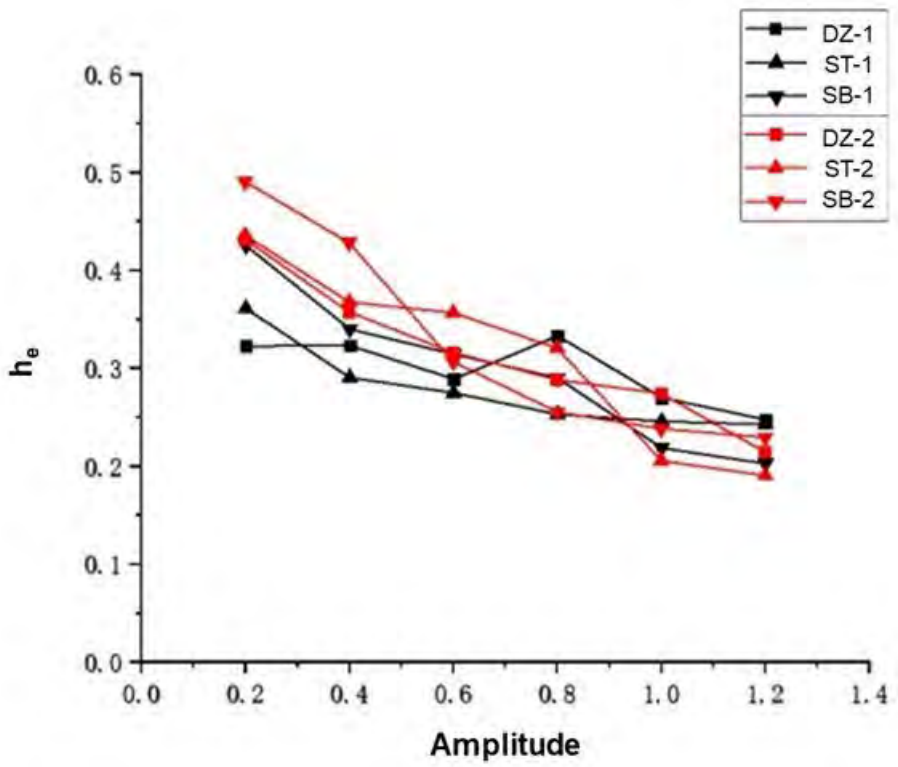


**Fig. 11.** The equivalent viscous damping coefficient curves of the mortise-tenon joints

Although the length and form of the mortise-tenon joints were different, the variation law of equivalent viscous damping coefficients were similar, which decreased with the increasing of the displacement amplitude. In the early stage of loading, when the specimens entered the failure stage, the energy consumption slowly decreased, and the energy consumption of some joints slightly increased. This was because in the early stage of loading, the mortise-tenon joint was subjected to pressure continuously. After plastic deformation, with the increase of the displacement amplitude, the deformation gradually decreased, and the ability of energy dissipation also gradually decreased. When the mortise-tenon joint was continuously loaded and entered the failure stage, the strong extrusion force cleaved the wood fibers, and the energy consumption capacity of the mortise-tenon members was slightly improved. As a whole, the equivalent damping coefficient of the mortise-tenon joints with a 'Que-Ti' component was larger and the energy dissipation capacity was better. Especially in the early stage of the test, it could be seen that the energy dissipation curve of each joint was higher, and the energy dissipation capacity was enhanced. When the displacement amplitude increased and the rotation angle increased, the displacement gradually increased, and the energy consumption of all the joints obviously decreased.

## CONCLUSIONS

1. Among the three mortise-tenon joints (straight-tenon joint, through-tenon joint, and half-tenon joint), the straight-tenon joint had the strongest bearing capacity.

2. Due to the asymmetry of the tenon form between the through-tenon joint and half-tenon joint, its hysteresis loop also presented asymmetric characteristics. Among the three joints, the half-tenon joint is most likely to pull out.
3. After adding the 'Que-Ti' components, the tenon pulling situation of the half-tenon joint can be effectively alleviated. From the perspective of energy consumption, it was determined that the energy consumption capacity of the mortise-tenon joints after adding a 'Que-Ti' was stronger than the energy consumption capacity of the mortise-tenon joints without a 'Que-Ti', which also shows that the 'Que-Ti' component can be used as an effective component to enhance the mechanical properties of mortise-tenon joints.

## ACKNOWLEDGMENTS

Special thanks to following for their research support: the National Natural Science Foundation of China (31860184); the Young Talents of Science and Technology in Universities of Inner Mongolia Autonomous Region (NJYT-20-A15); the Inner Mongolia science and technology major projects (CGZH2018135); and the Inner Mongolia grassland talent team, innovation talent team (TC2019071720712).

## REFERENCES CITED

Chun, Q., Yue, Z., and Pan, J. (2011). "Experimental study on seismic characteristics of typical mortise-tenon joints of Chinese southern traditional timber frame buildings," *Science China Technological Sciences* 54(9), 2404- 2411. DOI: 10.1007/s11431-011-4448-3

Chun, Q., Jin, H., Dong, Y., Hua, Y., and Han, Y. (2019). "Research on mechanical properties of Dingtougong mortise-tenon joints of Chinese traditional hall-style timber buildings built in the Song and Yuan dynasties," *International Journal of Architectural Heritage* 14(5), 729-750. DOI: 10.1080/15583058.2019.1568613

Dai, L. (2020). "Finite-element model updating of the traditional beam-column joint in Tibetan heritage buildings using uniform design," *Advances in Structural Engineering* 23(9), 1890-1901. DOI: 10.1177/1369433220903984

Dong, H., He, M., Wang, X., Christopoulos, C., Li, Z., and Shu, Z. (2021). "Development of a uniaxial hysteretic model for dowel-type timber joints in OpenSees," *Construction and Building Materials* 288, 1-17. DOI: 10.1016/j.conbuildmat.2021.123112

Erdil, Y. Z., Kasal, A., and Eckelman, C. A. (2005). "Bending moment capacity of rectangular mortise and tenon furniture joints," *Forest Products Journal* 55(12), 209-213.

GB/T 1935 (2009). "Method of testing in compressive strength parallel to grain of wood," Standardization Administration of China, Beijing, China.

GB/T 1936.1 (2009). "Method of testing in bending strength of wood," Standardization Administration of China, Beijing, China.

GB/T 1939 (2009). "Method of testing in compression perpendicular to grain of wood," Standardization Administration of China, Beijing, China.

Hu, W., and Liu, N. (2020). "Numerical and optimal study on bending moment capacity and stiffness of mortise-and-tenon joint for wood products," *Forests* 11(5), 501. DOI: 10.3390/f11050501

Huang, H., Sun, Z., Guo, T., and Li, P. (2017). "Experimental study on the seismic performance of traditional Chuan-Dou style wood frames in southern China," *Structural Engineering International* 27(2), 246-254. DOI: 10.2749/101686617X14881932435817

ISO 16670 (2003). "Timber structures - Joints made with mechanical fasteners - Quasi-static reversed-cyclic test method," International Organization for Standardization, Geneva, Switzerland.

Li, S., Zhou, Z., Luo, H., Milani, G., and Abruzzese, D. (2020). "Behavior of traditional Chinese mortise - tenon joints: Experimental and numerical insight for coupled vertical and reversed cyclic horizontal loads," *Journal of Building Engineering* 30, 1-15. DOI: 10.1016/j.jobe.2020.101257

Likos, E., Haviarova, E., Eckelman, C. A., Erdil, Y. Z., and Ozcifci, A. (2012). "Effect of tenon geometry, grain orientation, and shoulder on bending moment capacity and moment rotation characteristics of mortise and tenon joints," *Wood and Fiber Science* 44(4), 462-469.

Loss, C., Tannert, T., and Tesfamariam, S. (2018). "State-of-the-art review of displacement-based seismic design of timber buildings," *Construction and Building Materials* 191, 481-497. DOI: 10.1016/j.conbuildmat.2018.09.205

Lyu, M., Zhu, X., and Yang, Q. (2016). "Connection stiffness identification of historic timber buildings using temperature-based sensitivity analysis," *Engineering Structures* 131, 180-191. DOI: 10.1016/j.engstruct.2016.11.012

Lyu, M., Zhu, X., and Yang, Q. (2017). "Bilinear connection stiffness identification of heritage timber buildings with limited strain measurements," *Engineering Structures* 151, 665-681. DOI: 10.1016/j.engstruct.2017.08.058

Meng, Z., Li, T., and Yang, Q. (2019). "Experimental study on the seismic mechanism of a full-scale traditional Chinese timber structure," *Engineering Structures* 180, 484-493. DOI: 10.1016/j.engstruct.2018.11.055

Poletti, E., Vasconcelos, G., Branco, J. M., and Isopescu, B. (2019). "Effects of extreme environmental exposure conditions on the mechanical behaviour of traditional carpentry joints," *Construction and Building Materials* 213, 61-78. DOI: 10.1016/j.conbuildmat.2019.04.030

Prekrat, S., and Smardzewski, J. (2010). "Effect of glue line shape on strength of mortise and tenon joint," *Drvna Industrija* 61(4), 223-228.

Tankut, A. N., and Tankut, N. (2005). "The effects of joint forms (shape) and dimensions on the strengths of mortise and tenon joints," *Turkish Journal of Agriculture and Forestry* 29, 493-498.

Wang, X. L., and Jin, L. (2014). "Analysis of the influence of mortise-tenon joint damage on seismic performance of ancient timber structure," *Applied Mechanics and Materials* 580-583, 1595-1599. DOI: 10.4028/www.scientific.net/AMM.580-583.1595

Wilczyński, A., and Warmbier, K. (2003). "Effect of joint dimensions on strength and stiffness of tenon joints," *Folia Forestalia Polonica* 34, 53-66.

Xie, Q., Tong, Y., Zhang, L., Li, S., and Wang, L. (2019). "Seismic behavior of Chinese traditional timber frames with masonry infill wall: Experimental tests and hysteretic

model," *International Journal of Architectural Heritage* 15(8), 1130-1144. DOI: 10.1080/15583058.2019.1665140

Xie, Q., Wang, L., Li, S., Zhang, L., and Hu, W. (2020). "Influence of wood infill walls on the seismic performance of Chinese traditional timber structure by shaking table tests," *Bulletin of Earthquake Engineering* 18(10), 5009-5029. DOI: 10.1007/s10518-020-00886-0

Xue, J., and Xu, D. (2018). "Shake table tests on the traditional column-and-tie timber structures," *Engineering Structures* 175, 847-860. DOI: 10.1016/j.engstruct.2018.08.090

Xue, J., Xu, D., and Xia, H. (2018). "Experimental study on seismic performance of through-tenon joints with looseness in ancient timber structures," *International Journal of Architectural Heritage* 14(4), 483-495. DOI: 10.1080/15583058.2018.1552996

Xue, J., Guo, R., Qi, L., and Xu, D. (2019). "Experimental study on the seismic performance of traditional timber mortise-tenon joints with different looseness under low-cyclic reversed loading," *Advances in Structural Engineering* 22(6), 1312-1328. DOI: 10.1177/1369433218814167

Yang, Q., Lyu, M., and Zhu, X. (2020). "Nonlinear connection stiffness identification of heritage timber buildings using a temperature-driven multi-model approach," *International Journal of Structural Stability and Dynamics* 20(10), 1-28. DOI: 10.1142/S0219455420420018

Yue, Z. (2014). "Traditional Chinese wood structure joints with an experiment considering regional differences," *International Journal of Architectural Heritage: Conservation, Analysis, and Restoration* 8(2), 224-246. DOI: 10.1080/15583058.2012.688179

Záborský, V., Borůvka, V., Kašičková, V., and Ruman, D. (2017). "Effect of wood species, adhesive type, and annual ring directions on the stiffness of rail to leg mortise and tenon furniture joints," *BioResources* 12(4), 7016-7031. DOI: 10.15376/biores.12.4.7016-7031

Article submitted: March 28, 2022; Peer review completed: April 30, 2022; Revised version received and accepted: May 12, 2022; Published: May 17, 2022.
DOI: 10.15376/biores.17.3.4116-4135